Journal of Geotechnical Engineering
Research paper
Vol 11,issue 1,2024
Receiving date:01-4-2024
Acceptance date:10-4-2024
Publication date:13-4-2024

Spatial variations of land surface temperature and its relationship with the type of land use/cover

Asra Fathi[a], Ali Khazai[a], Fereshteh Doostvandi[a*]

[a] Department of Geography, Razi University, Kermanshah-Iran (Corresponding author: f.dostvandi@gmail.com)

Abstract:

Environmental parameters are intricately interdependent and affect nearby and sometimes distant components. Environmental parameters become more important when dealing directly with humans. Land surface temperature (LST) is one of the environmental parameters that when it is related to the city as the main center of human gathering, it is referred to as urban heat island (UHI). Land use/ Land cover (LU/LC) is one of the important environmental parameters that affect the temperature of the earth's surface and heat island. In this research, using the Landsat 8 satellite image, the effect of LULC on the LST of Kermanshah and its outskirts was investigated. For this purpose, first the required pre-processing was done on the image of the desired date; Single-channel algorithm was used to prepare LST map and maximum likelihood algorithm was used to prepare LULC map. The temperature of the studied area was between 25 and 63 degrees Celsius. Among the five extracted LULC classes (water, vegetation, built, soil and rock), vegetation had the lowest average temperature (44.6 degrees Celsius) and soil had the highest average temperature (54.7 degrees Celsius). The reason why the temperature of the built areas was not high was the reflective roofs and the reason why the water temperature was not low (compared to the vegetation) was mixed pixels.

Key words: thermal island, LST, LULC, reflective roofs, Kermanshah city

Introduction:

Land surface temperature (LST) is the temperature of the earth's surface crust, which is a key parameter for land surface processing studies at regional and global scales. LST is crucial for understanding surface energy balance and urban climatology, influenced by characteristics such as vegetation type, land use-land cover, and surface impermeability. The continuous expansion

Journal of Geotechnical Engineering
Research paper
Vol 11,issue 1,2024
Receiving date:01-4-2024
Acceptance date:10-4-2024
Publication date:13-4-2024

of urban areas has significantly altered land surfaces, leading to substantial changes in LST. Research concerning LST and advancements in technology play a pivotal role in urban climate studies[1-10].

With over half of the world's population residing in urban areas, a figure projected to rise to nearly 70% by 2050, the phenomenon of urban heat islands (UHI) has gained prominence. UHI refers to the disparity in temperature between built-up urban areas and adjacent rural regions, attributable to increased heat storage capacity in cities. This temperature differential negatively impacts air quality, energy consumption, biological systems, and human health[11-15].

Advancements in thermal remote sensing, geographic information systems (GIS), and statistical methods have enabled researchers to analyze the relationship between UHI and the landscape. Thermal infrared remote sensing (TIR) serves as a primary method for acquiring LST data on a large scale. However, mitigating the effects of UHI based solely on spatial LST patterns remains challenging, necessitating a deeper understanding of the quantitative relationship between LST and various contributing factors[16-19].

Concerns regarding land-use/cover change have been a focal point in global environmental change research. It's been recognized that alterations in land cover impact surface albedo and subsequently influence surface-atmosphere energy exchange, thereby affecting regional climates. Detailed land use mapping and forecasting facilitate informed planning processes. Investigating the influence of land use/cover classes on surface temperature distribution in urban areas is crucial for contemporary studies. Therefore, this study examines the role of land use/cover classes in shaping the spatial distribution of surface temperature in Kermanshah city and its environs[20-25].

Methodology:

Study area:

Kermanshah city with an approximate area of 5759 square kilometers (approximately 23.1% of the area of Kermanshah province) in terms of geographical location between latitudes 34 degrees and 47 minutes to 34 degrees and 48 minutes north and longitudes 47 degrees and 30 minutes to 47 degrees and 32 minutes east is located in the middle part of Kermanshah province. Kermanshah city is the center of this city and the most important city in the central region of western Iran.

Journal of Geotechnical Engineering
Research paper
Vol 11,issue 1,2024
Receiving date:01-4-2024
Acceptance date:10-4-2024
Publication date:13-4-2024

Kermanshah city is located between latitudes 34 degrees and 15 minutes to 34 degrees and 24 minutes north and longitudes 46 degrees and 59 minutes to 47 degrees and 12 minutes east. The height of the city from the sea level is 1322 and its area is about 88 square kilometers (Nasariyeh, 2015). Figure 1 shows the studied area.

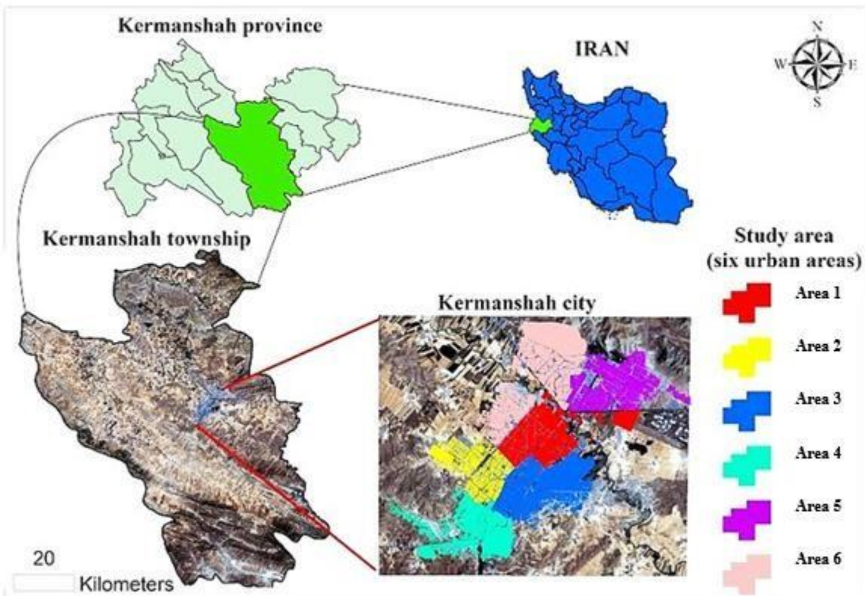

Figure (1): Map of the study area (Zinatizadeh et al 2017)

This research was conducted with the aim of investigating the effect of land use/cover on the changes in the surface temperature of the earth. For this purpose, Landsat TM OLI satellite images were downloaded and used in 2022. Additional information about the image used is provided in Table 1.

Table (1): images used Information

Row	Path	Date	Sensor
36	167	2022.08.13	OLI

The first step for conducting this study is the registration process so that the images are spatially matched and the analyzes are more valid. for this purpose; Some specific coordinates in the image were matched with Google Earth images. In the following, the steps of converting the raw images of OLI sensors to the temperature of the earth's surface will be described.

Journal of Geotechnical Engineering
Research paper
Vol 11,issue 1,2024
Receiving date:01-4-2024
Acceptance date:10-4-2024
Publication date:13-4-2024

1. Digital number to radiance

The conversion of gray levels to radiance is actually the internal calibration of the meter. The raw data recorded by the detectors have a linear response with the Earth's brightness, this response is converted to 8-bit (for Landsat 5) and 16-bit (for Landsat 8) data. By using relation 1 and the information in the metadata that can be obtained along with downloading the images, the raw images were converted into radiance images.

$$L_{\lambda} = \text{gain} \times \text{QCAL} + \text{offset} \tag{1}$$

Where, Lλ is the amount of radiance in watts per square meter per steradian per micrometer (W.m-2.str-1μm-1) and QCAL is the gray level in the desired pixel. The values of gain and offset are the slope and width from the origin, respectively, which can be extracted from the metadata information.

2. Atmospheric correction

By converting the digital number (DN) to reflectance top of atmosphere (TOA) and surface reflectance, the atmospheric effects on the reflected wavelengths are removed so that the desired indices can be extracted for use. For this purpose, the FLAASH algorithm [26-30]

3. Calculation of brightness temperature:

After obtaining the spectral radiance of the data, equation 2 is used to convert the radiance to the brightness temperature.

$$T = \frac{K2}{In(\frac{K1}{L\lambda}+1)} \tag{2}$$

In this regard, Lλ means the amount of radiance in watts per square meter per stradian per micrometer (W.m-2.str-1μm-1) and k1 and k2 for Landsat 5 and Landsat 8 sensors are according to Table 2.

Table (2): The amount of k1 and k2 in the Landsat 8

k_2(Kelvin)	(W.m-2.str-1μm-1)k_1	K / Band
1321.0789	774.8853	Band 10
1201.1442	480.8883	Band 10

Journal of Geotechnical Engineering
Research paper
Vol 11,issue 1,2024
Receiving date:01-4-2024
Acceptance date:10-4-2024
Publication date:13-4-2024

4. Calculation of the emissivity coefficient of the earth's surface

The surface emissivity coefficient (LSE) is an index of the surface's inherent efficiency in converting thermal energy into radiant energy above the surface, which depends on the composition, roughness, moisture content of the surface, and observation conditions (such as wavelength, pixel magnification, and viewing angle). There are different ways to get LSE. One of these methods is obtaining LSE from NDVI [31-37]. In this method, LSE is calculated from equation 3.

$$\varepsilon = \varepsilon_{veg} P_v + \varepsilon_{soil} (1+P_v) \qquad (3)$$

In this relation, εveg and εsoil for this gauge are presented in Table 3 and Pv is calculated from Equation 4.

Table (3) amount of εveg and εsoil for the meter used

ε_{soil}	ε_{veg}	Band
0.9863	0.9668	Band 10
0.9896	0.9747	Band 11

$$\text{NDVI} = \frac{NDVI - NDVI_{min}}{NDVI_{max} - NDVI_{min}} \qquad (4)$$

In this regard, NDVImin and NDVImax mean the lowest and highest NDVI values respectively (usually soil and vegetation).

5. Land surface temperature (LST)

The single-channel (SC) algorithm used to retrieve LST from Landsat satellite thermal images in this research, the algorithm developed by James-Moons et al. 2014 has been applied on Landsat 8. This algorithm is applied to all Landsat in the same way and with the relation 5.

$$T_S = \gamma \left[\frac{1}{\varepsilon} \left(\psi_1 L_{sen} + \psi_2 \right) + \psi_3 \right] + \delta \qquad (5)$$

In this, Ts is the land surface temperature, ε is the radiant power of the earth's surface, and Lsen is the radiance on the measuring surface. The parameters λ and δ are obtained from the relation 6.

Journal of Geotechnical Engineering
Research paper
Vol 11,issue 1,2024
Receiving date:01-4-2024
Acceptance date:10-4-2024
Publication date:13-4-2024

$$\gamma \approx \frac{{T_{sen}}^{2}}{b_{\gamma} L_{sen}}; \qquad \delta \approx T_{sen} - \frac{{T_{sen}}^{2}}{b_{\gamma}} \tag{6}$$

where, Tsen is the luminance temperature of the measuring surface, bγ=C2/λ and 1Ψ, 2Ψ and 3Ψ functions are atmospheres obtained according to relation 7 (Jiménez-Muñoz et al., 2014; Maleki et al., 2019).

$$\psi 1 = 1/\tau \; ; \; \psi 2 = -Ld - Lu/\tau \; ; \; \psi 3 = Ld. \tag{7}$$

Image classification:

Remote sensing research focusing on image classification has long attracted the attention of the remote sensing community because classification results are the basis for many environmental and socio-economic applications. Scientists have put a lot of effort into developing advanced classification methods and techniques to improve classification accuracy. Classification of remote sensing is a complex process and requires consideration of many factors. The choice of data type depends on the purpose of the research, the economic conditions of the project, the desired scale, and other factors[37-41].

Based on the studies, the maximum likelihood algorithm assumes that the reflection values of each class have a normal (Gaussian) distribution in each band, and the MLC algorithm assigns a pixel to the class with the highest probability. The pixel probability is analyzed by the multivariate normal cumulative distribution function (CDF) through the mean, variance, and covariance of the training samples. The MLC equation is shown in formula (8).

$$P(x|w_i) = \frac{1}{\frac{n}{((2\pi)|V_i|0.5)}} \exp[-0.5(X - M_i)^T {V_i}^{-1}(X - M_i)] \tag{8}$$

where:

n = number of multispectral bands,

X = unknown measurement vector,

Vi = covariance matrix for each class,

M = mean vector of each training class.

Journal of Geotechnical Engineering
Research paper
Vol 11,issue 1,2024
Receiving date:01-4-2024
Acceptance date:10-4-2024
Publication date:13-4-2024

Results:

In this section, the results of applying the methods to the used data and examining the relationship between land cover use and ground surface temperature in Kermanshah city and its suburbs are discussed. The items presented in this chapter include:

1 land use map in 2022

2 accuracy table of land use map production

3 graphs of each of the land cover use classes

4 Earth surface temperature map

5 diagram of the area of temperature classes

6 graphs of the average temperature of each classis

Figure 2 shows the land use map of Kermanshah city and its suburbs. The land use map in 5 layers of built-up areas (buildings, roads, etc.), rock layer, bare soil, vegetation (agriculture/gardens and vegetation) natural) and water is prepared.

At first glance, it is the part where the most area of the area is bare soil, and then the most areas are related to the stone/rock and built classes, and finally, water use has the lowest level.

Journal of Geotechnical Engineering
Research paper
Vol 11,issue 1,2024
Receiving date:01-4-2024
Acceptance date:10-4-2024
Publication date:13-4-2024

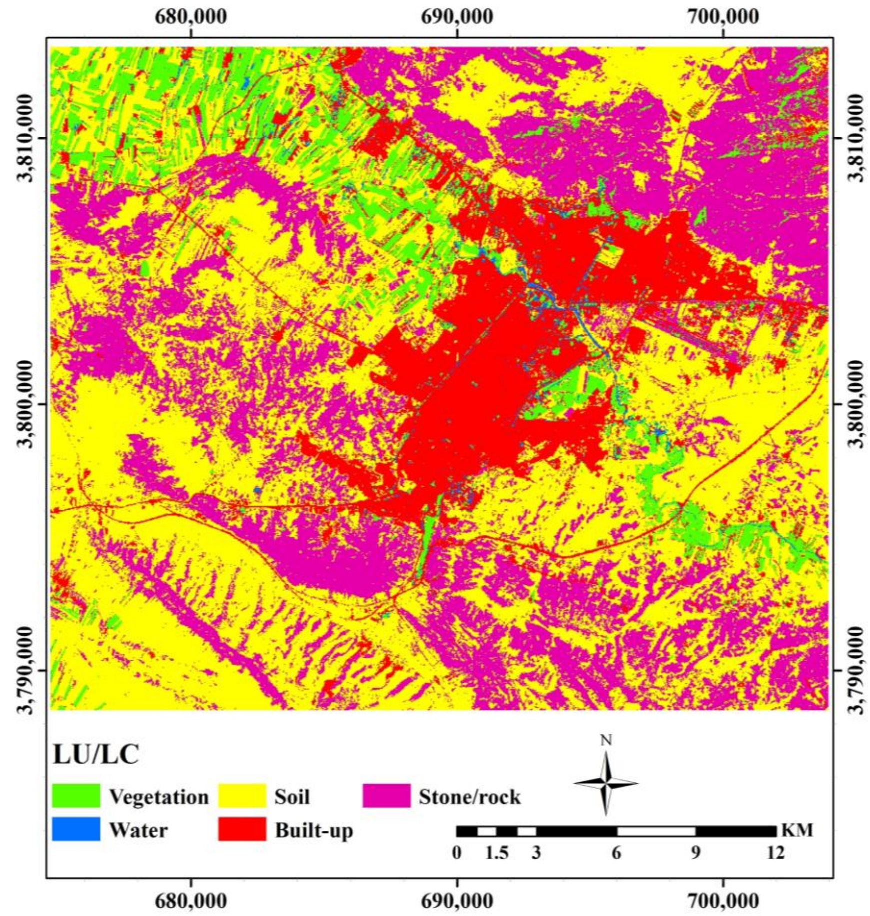

Figure (2): land use/ land cover map

Table 4, the information related to the accuracy of the land use map produced according to the information in this table, the overall accuracy is more than 91% and the kappa coefficient is more than 90%, indicating the high accuracy of the land use map production. The only cover user whose usage accuracy is 68% regarding water and in other cases the accuracy is above 90%.

Table (4): accuracy of production of land use map

LU/LC	producer accuracy	User accuracy	Omission error	Commission error	overall accuracy	kappa coefficient
Vegetation	94.33	97.92	5.67	2.08		
Water	90.8	67.27	9.2	32.73		

Journal of Geotechnical Engineering
Research paper
Vol 11,issue 1,2024
Receiving date:01-4-2024
Acceptance date:10-4-2024
Publication date:13-4-2024

Built-Up	93.98	98.28	6.02	1.72	91.64	90.37
Soil	96.85	97.98	3.15	2.02		
rock/stone	98.93	96.77	1.07	3.23		

Figure 3 shows the area diagram of each of the LULC. According to this diagram, soil covers the largest area of the region with 341 square kilometers, and water use covers the lowest area with 6.9 square kilometers. Built-up land use areas, with about 113 square kilometers, are the third land use in terms of area.

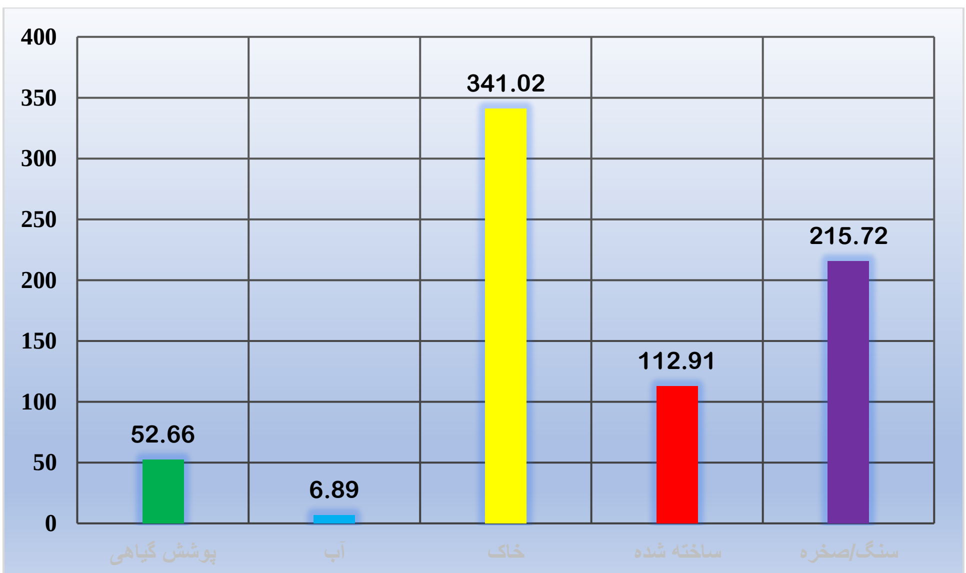

Figure (3): Diagram of the area of LULC classes

Figure 4 shows the surface temperature map of the studied area. Based on this figure, most of the area has a temperature of more than 55 degrees (to 63 degrees) Celsius

The interesting thing is that the temperature in the city limits is often lower than the suburbs and the prevailing temperatures in the city limits are between 40-45 and 25-40.

Journal of Geotechnical Engineering
Research paper
Vol 11,issue 1,2024
Receiving date:01-4-2024
Acceptance date:10-4-2024
Publication date:13-4-2024

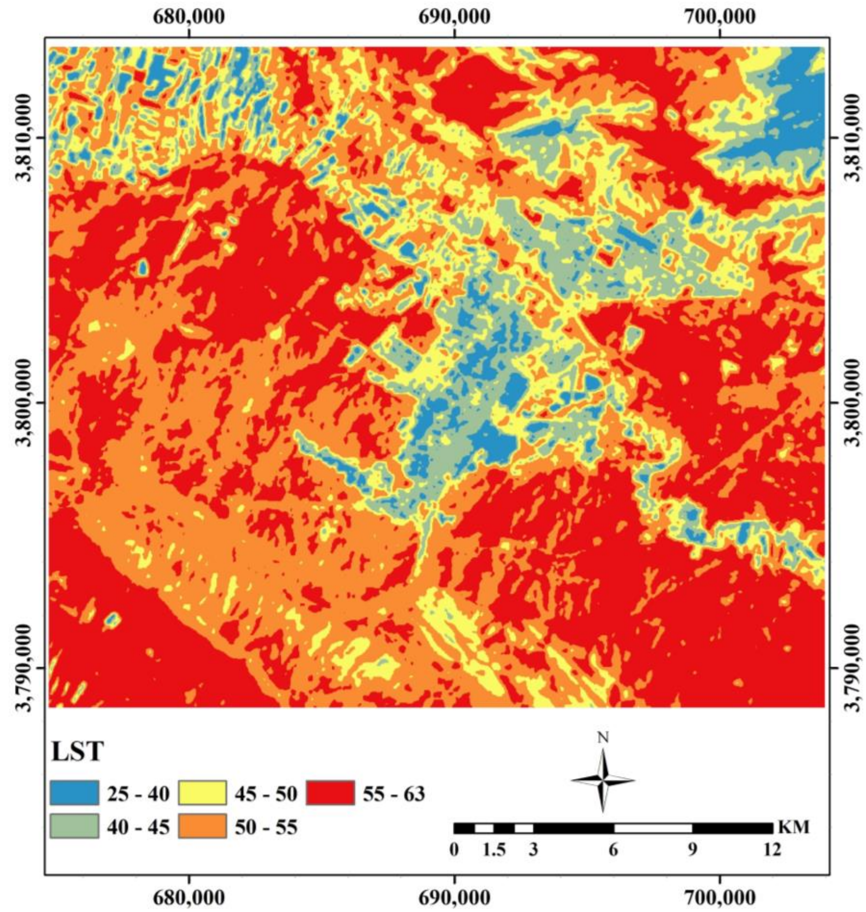

Figure (4): Land surface temperature map

Figure 5 is the diagram of the area of temperature classes. Contrary to imagination, the area of the 55–63 degree class is not much different from the 55-55 degree classes. (Less than 3 square kilometers). According to this diagram, the 55–63-degree class has the largest area with 268 square kilometers, and the area covered by the classes decreases accordingly. So that 25–40-degree classes have covered the least area with 27.6 square kilometers.

Journal of Geotechnical Engineering
Research paper
Vol 11,issue 1,2024
Receiving date:01-4-2024
Acceptance date:10-4-2024
Publication date:13-4-2024

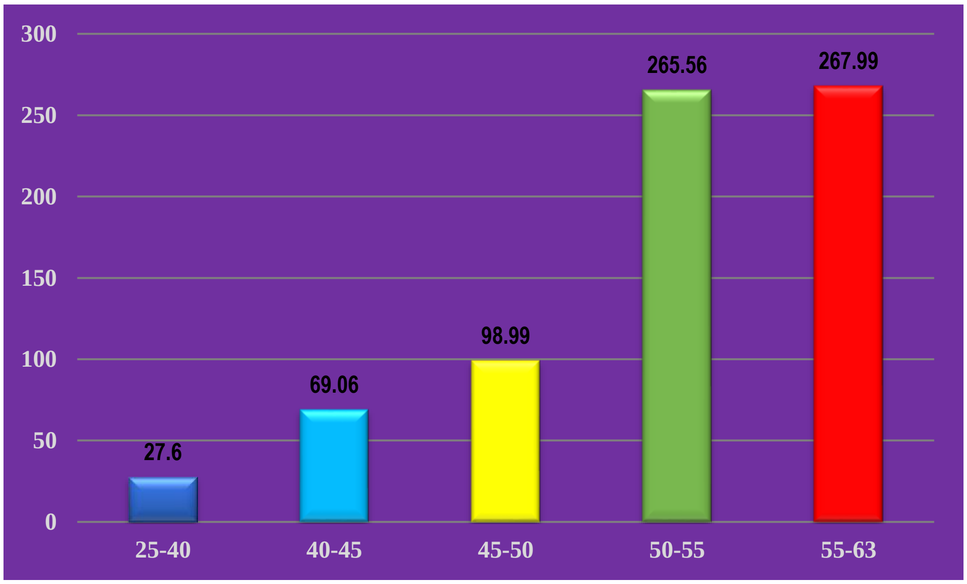

Figure (5): Diagram of the area of temperature classes

Figure 6 is the graph of average temperature of LULC classes. According to this graph, the lowest average temperature is related to vegetation with 6.44 degrees Celsius. Then water usage with 4.46 degrees Celsius has the second average temperature**.**

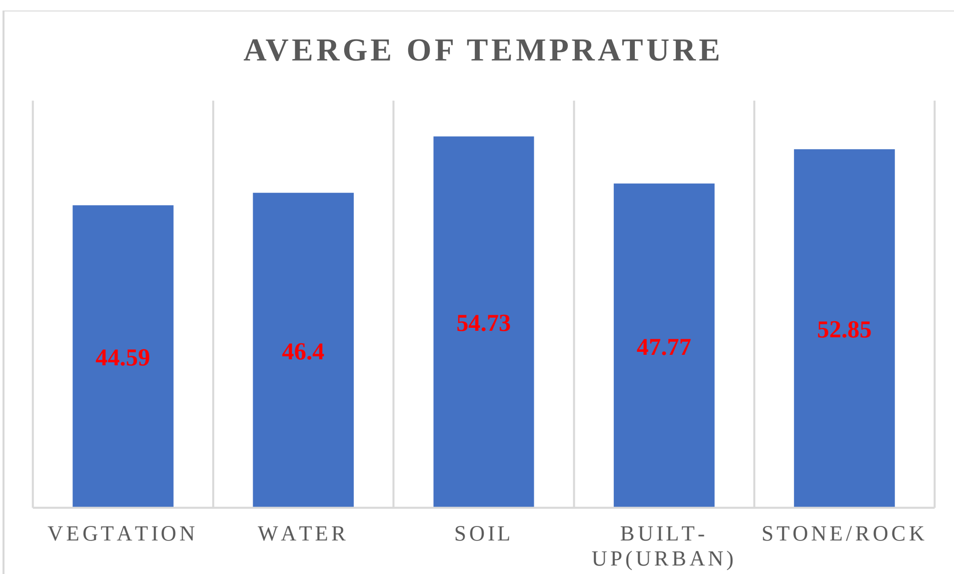

Figure (6): Average temperature diagram of land use/cover classes

Journal of Geotechnical Engineering
Research paper
Vol 11,issue 1,2024
Receiving date:01-4-2024
Acceptance date:10-4-2024
Publication date:13-4-2024

On the opposite side, soil cover has the highest average temperature with 7.54 degrees. Due to the fact that the land use/water cover has low accuracy and also because it has a small area that is mostly in a narrow linear shape and includes mixed pixels, the temperature of this land use is higher than the vegetation temperature in the study area.

Conclusion:

In this study, Landsat satellite images and especially Landsat 8 (OLI) were used to check the map of land use/cover classes in the spatial distribution of surface temperature in Kermanshah city and its limits. To prepare the land use map, the maximum likelihood algorithm was used, and based on the results of the studies of Zare-Naghdehai et al. (2021), this algorithm has a suitable capability for land cover use classification. The results of this study in this section confirmed the results of their study and showed that this algorithm has a good ability to detect LULC According to the results of Table 4, it is clear that the accuracy is often higher than 95% and the error rate is less than 5%. Only in the case of water LULC and more specifically the error of commission and the other side of that is the accuracy of the user, where the amount of error of commission is high (32.73 percent) and the amount of accuracy of the user is relatively low (67.27 percent); This problem is due to the limitations of access to ground reference data, especially in this LULC, and the resolution of free images, as well as the small extent of blue areas, causes the creation of mixed pixels. The commission error rate was high and the user accuracy rate was low.

Land surface temperature is an important parameter in environmental studies, which affects not only humans, but also living organisms and even natural environments such as plants, water bodies, etc. LULC is known as one of the effective parameters on the spatial changes of the earth's surface temperature. The results of this study in the city of Kermanshah and the impact of 5 types of LULC in the city of Kermanshah showed that the use of vegetation has the lowest average temperature (about 44.6 degrees Celsius). Regarding the results of this research, three points are noteworthy and worth checking: 1. The temperature of water is 1.8 degrees Celsius higher than that of vegetation, due to the fact that water has a high specific heat capacity (which means that it heats up later and cools down later). Considering that at 10:15 a.m. the water temperature has not yet risen completely, it seems that this amount is a bit high, which can be attributed to the lower validity of this LULC (mixing it with urban use and buildings); Therefore, it requires more studies in this field. 2. Contrary to the notion and assumptions regarding the urban heat island, the map in Figure 4 shows that generally urban areas have a lower temperature, which is due to the effects of reflective roofs (Hashmi Dere Badami et al., 2014). 3. The third point, the high average temperature of the soil and stone indicates that the reason for the high temperature felt in the outskirts of the cities (which is under construction and preparing the land for construction, generally with the destruction natural areas and their transformation into bare soil) is due to the

Journal of Geotechnical Engineering
Research paper
Vol 11,issue 1,2024
Receiving date:01-4-2024
Acceptance date:10-4-2024
Publication date:13-4-2024

high absorption of temperature in these uses, although they do not have the conditions of trapped heat in urban areas, but they generally have high temperatures.

References:

1. *Alavipanah, K., Khazai, A., & Hashemidarebadami, S. (2015). Assessment of influence of reflective roofs on reducing urban heat island effect by satellite images (A case study in Kermanshah). Journal of Urban-Regional Studies and Research, 7(25), 1-18.*
2. *Bakhshi Lomer, A. R., Rezaeian, M., Rezaei, H., Lorestani, A., Mijani, N., Mahdad, M., ... & Arsanjani, J. J. (2023). Optimizing Emergency Shelter Selection in Earthquakes Using a Risk-Driven Large Group Decision-Making Support System. Sustainability, 15(5), 4019.*
3. *Felde, G. W., Anderson, G. P., Cooley, T. W., Matthew, M. W., Berk, A., & Lee, J. (2003, July). Analysis of Hyperion data with the FLAASH atmospheric correction algorithm. In IGARSS 2003. 2003 IEEE International Geoscience and Remote Sensing Symposium. Proceedings (IEEE Cat. No. 03CH37477) (Vol. 1, pp. 90-92). IEEE.*
4. *Ghanbari, R., & Borna, K. (2021, March). Multivariate time-series prediction using LSTM neural networks. In 2021 26th International Computer Conference, Computer Society of Iran (CSICC) (pp. 1-5). IEEE.*
5. *Ghanbari, R., Heidarimozaffar, M., Soltani, A., & Arefi, H. (2023). Land surface temperature analysis in densely populated zones from the perspective of spectral indices and urban morphology. International Journal of Environmental Science and Technology, 1-20.*
6. *Grimmond, S. (2007). Urbanization and global environmental change: local effects of urban warming. The Geographical Journal, 173(1), 83-88.*
7. *Hashmi, S., Maleki, M., Jomezade, B., Hazeh, S., & Bagheri, K. (2019). Potential Evaluation of SMA and NSMA Methods Implementation to Extract Sub-pixel Impervious Surfaces from Landsat 8 Imagery (OLI), (Case Study: Sari). Geographic Thought, 10(20), 115-138.*
8. *Jiménez-Muñoz, J. C., Sobrino, J. A., Skoković, D., Mattar, C., & Cristobal, J. (2014). Land surface temperature retrieval methods from Landsat-8 thermal infrared sensor data. IEEE Geoscience and remote sensing letters, 11(10), 1840-1843.*
9. *Khandelwal, S., Goyal, R., Kaul, N., & Mathew, A. (2018). Assessment of land surface temperature variation due to change in elevation of area surrounding Jaipur, India. The Egyptian Journal of Remote Sensing and Space Science, 21(1), 87-94.*
10. *Lambin, E. F., Geist, H. J., & Lepers, E. (2003). Dynamics of land-use and land-cover change in tropical regions. Annual review of environment and resources, 28(1), 205-241.*
11. *Lhissou, R., El Harti, A., Maimouni, S., & Adiri, Z. (2020). Assessment of the image-based atmospheric correction of multispectral satellite images for geological mapping in arid and semi-arid regions. Remote Sensing Applications: Society and Environment, 20, 100420.*

Journal of Geotechnical Engineering
Research paper
Vol 11,issue 1,2024
Receiving date:01-4-2024
Acceptance date:10-4-2024
Publication date:13-4-2024

12. *Li, Y., Zhao, M., Mildrexler, D. J., Motesharrei, S., Mu, Q., Kalnay, E., ... & Wang, K. (2016). Potential and actual impacts of deforestation and afforestation on land surface temperature. Journal of Geophysical Research: Atmospheres, 121(24), 14-372.*
13. *Maduako, I. D., Yun, Z., & Patrick, B. (2016). Simulation and prediction of land surface temperature (LST) dynamics within Ikom City in Nigeria using artificial neural network (ANN). Journal of Remote Sensing & GIS, 5(1), 1-7.*
14. *Maleki, M., Ahmadi, Z., & Dosti, R. (2019). Kermanshah land surface temperature changes in during 1393-1397 periods. Geography and Human Relationships, 2(3), 309-319.*
15. *Maleki, M., Tavakkoli Sabour, S. M., Zeaieanfirouzabadi, P., & Raeisi, M. (2018). Comparison of optic and radar data for terrain feature extraction. Journal of RS and GIS for Natural Resources, 9(2), 93-107.*
16. *Maleki, M., Van Genderen, J. L., Tavakkoli-Sabour, S. M., Saleh, S. S., & Babaee, E. (2020). Land use/cover change in Dinevar rural area of West Iran during 2000–2018 and its prediction for 2024 and 2030. Geogr. Tech, 15, 93-105.*
17. *Mamdoohi, A. R., Rezaei, H., Irannezhad, E., Saffarzadeh, A., & Abbasi, M. (2022). Hour-and Period-based congestion pricing, case of Tehran mode choice. Quarterly Journal of Transportation Engineering.*
18. *Meineke, E. K., Dunn, R. R., & Frank, S. D. (2014). Early pest development and loss of biological control are associated with urban warming. Biology letters, 10(11), 20140586.*
19. *Mo, Y., Xu, Y., Chen, H., & Zhu, S. (2021). A review of reconstructing remotely sensed land surface temperature under cloudy conditions. Remote Sensing, 13(14), 2838.*
20. *Naserieh, M (2015). Investigating temporal-spatial changes of Kermanshah thermal island and its relationship with air pollution using satellite images, Master's Thesis, Department of Geography, Razi University.*
21. *Neinavaz, E., Skidmore, A. K., & Darvishzadeh, R. (2020). Effects of prediction accuracy of the proportion of vegetation cover on land surface emissivity and temperature using the NDVI threshold method. International Journal of Applied Earth Observation and Geoinformation, 85, 101984.*
22. *Oke, T. R. (1982). The energetic basis of the urban heat island. Quarterly Journal of the Royal Meteorological Society, 108(455), 1-24.*
23. *Otterman, J. (1974). Baring high-albedo soils by overgrazing: a hypothesized desertification mechanism. Science, 186(4163), 531-533.*
24. *Peng, J., Jia, J., Liu, Y., Li, H., & Wu, J. (2018). Seasonal contrast of the dominant factors for spatial distribution of land surface temperature in urban areas. Remote sensing of Environment, 215, 255-267.*
25. *Phan, T. N., & Kappas, M. (2018). Application of MODIS land surface temperature data: a systematic literature review and analysis. Journal of Applied Remote Sensing, 12(4), 041501-041501.*
26. *Plocoste, T., Jacoby-Koaly, S., Molinié, J., & Petit, R. H. (2014). Evidence of the effect of an urban heat island on air quality near a landfill. Urban Climate,10, 745-757.*

Journal of Geotechnical Engineering
Research paper
Vol 11,issue 1,2024
Receiving date:01-4-2024
Acceptance date:10-4-2024
Publication date:13-4-2024

27. *Rezaei, H., Irannezhad, E., & Mamdoohi, A. R. (2021). Heterogeneous analysis of mode choice behavior using latent class model. Journal of Transportation Research, 18(3), 61-74.*
28. *Rizwan, A. M., Dennis, L. Y., & Chunho, L. I. U. (2008). A review on the generation, determination and mitigation of Urban Heat Island. Journal of Environmental Sciences, 20(1), 120-128.*
29. *Sadidi, J., Maleki, M., Rahmati, M., & TAVAKKOLI, S. M. (2016). Investigating the Role of Faults in the Establishment and Survival of Settlements using Remote Sensing and Geographic Information System (GIS). The Case of Sahneh County in Iran. Journal of Settlements and Spatial Planning, 7(2), 201-206.*
30. *Saffarzadeh, M., Rezaei, H., & Majidi, M. Z. (2022). a Pricing Model for Freeway Tolls Based on the Share of Mode Shift, Route Shift, Travel Time Change and Users' Willingness to Pay (Case study: Tehran_Saveh Freeway). Journal of Transportation Research, 19(3), 359-370.*
31. *Sagan, C., Toon, O. B., & Pollack, J. B. (1979). Anthropogenic albedo changes and the earth's climate. Science, 206(4425), 1363-1368.*
32. *Sahani, N., Goswami, S. K., & Saha, A. (2021). The impact of COVID-19 induced lockdown on the changes of air quality and land surface temperature in Kolkata city, India. Spatial Information Research, 29, 519-534.*
33. *Tologbonse, E. B., Jibrin, M. M., Auta, S. J., & Damisa, M. A. (2013). Factors influencing women participation in women in agriculture (WIA) programme of Kaduna state agricultural development project, Nigeria. International Journal of Agricultural Economics and Extension, 1(7), 47-54.*
34. *Tran, D. X., Pla, F., Latorre-Carmona, P., Myint, S. W., Caetano, M., & Kieu, H. V. (2017). Characterizing the relationship between land use land cover change and land surface temperature. ISPRS Journal of Photogrammetry and Remote Sensing, 124, 119-132.*
35. *United Nations, 2010. World urbanization prospects: The 2009 revision population database. http://esa.un.org/unpd/wup/index.htm.*
36. *Valor, E., & Caselles, V. (1996). Mapping land surface emissivity from NDVI: Application to European, African, and South American areas. Remote sensing of Environment, 57(3), 167-184.*
37. *Wan, Z., Zhang, Y., Zhang, Q., & Li, Z. L. (2004). Quality assessment and validation of the MODIS global land surface temperature. International journal of remote sensing, 25(1), 261-274.*
38. *Yang, B., Yang, X., Leung, L. R., Zhong, S., Qian, Y., Zhao, C., ... & Qi, J. (2019). Modeling the impacts of urbanization on summer thermal comfort: the role of urban land use and anthropogenic heat. Journal of Geophysical Research: Atmospheres, 124(13), 6681-6697.*
39. *Yang, J., Ren, J., Sun, D., Xiao, X., Xia, J. C., Jin, C., & Li, X. (2021). Understanding land surface temperature impact factors based on local climate zones. Sustainable Cities and Society, 69, 102818.*
40. *Zare Naghadehi, S., Asadi, M., Maleki, M., Tavakkoli-Sabour, S. M., Van Genderen, J. L., & Saleh, S. S. (2021). Prediction of Urban Area Expansion with Implementation of MLC, SAM and SVMs' Classifiers Incorporating Artificial Neural Network Using Landsat Data. ISPRS International Journal of Geo-Information, 10(8), 513.*

Journal of Geotechnical Engineering
Research paper
Vol 11,issue 1,2024
Receiving date:01-4-2024
Acceptance date:10-4-2024
Publication date:13-4-2024

41. *Zinatizadeh, S., Azmi, A., Monavari, S. M., & Sobhanardakani, S. (2017). Evaluation and prediction of sustainability of urban areas: A case study for Kermanshah city, Iran. Cities, 66, 1-9.*